Analysis of Errors Introduced by Geographic Coordinate Systems on Weather Numeric Prediction Modeling

Yanni Cao[1,2,4], Guido Cervone[1,2,4,5], Zachary Barkely[3], Thomas Lauvaux[3], Aijun Deng[3], and Alan Taylor[2]

[1]Goeinformatics and Earth Observation Laboratory, The Pennsylvania State University, University Park, PA
[2]Department of Geography, The Pennsylvania State University, University Park, PA
[3]Department of Meteorology, The Pennsylvania State University, University Park, PA
[4]Institute for CyberScience, The Pennsylvania State University, University Park, PA
[5]Research Application Laboratory, National Center for Atmospheric Research, Boulder CO

Correspondence to: Guido Cervone (cervone@psu.edu)

Abstract. Most atmospheric models, including the Weather Research and Forecasting (WRF), use a spherical geographic coordinate system to internally represent input data and perform computations. However, most Geographic Information System (GIS) input data used by the models are based on a spheroid datum because it better represents the actual geometry of the earth. WRF and other atmospheric models use these GIS input layers as if they were in a spherical coordinate system without accounting for the difference in datum.

When GIS layers are not properly reprojected, latitudinal errors of up to 21 km in the mid-latitudes are introduced. Recent studies have suggested that for very high resolution applications, the difference in datum in the GIS input data (e.g. terrain land use, orography) should be taken into account. However, the errors introduced by the difference in coordinate systems remain unclear. This research quantifies the effect of using spherical vs spheroid datum for the input GIS layers used by WRF to study greenhouse gas transport and dispersion in Northeast Pennsylvania.

1 Introduction

Geographic Information Science (GISc) datasets are usually projected on a spheroid Geographic Coordinate System (GCS) such as World Geodetic System 1984 (WGS84) or North American Datum 1983 (NAD83). The earth is an irregular oblate spheroid, and these datums are used to better approximate the actual shape of the planet, which is flattened at the poles and bulged at the equator. The datums are used in combination with different projections (e.g. Universal Transverse Mercator (UTM), Lat-Lon, Albert Equal Area) to map a 3D view of the earth onto a 2D plane.

Atmospheric models are based on a spherical coordinate system because it usually leads to faster computations and an easier representation of data (Monaghan et al., 2013). The GISc layers used as input data for the atmospheric models generally use a spheroid datum, but they are ingested by the models as if they used spherical datums. Using different GCSs can affect the model results because the input data are mapped to different locations. This difference can lead to latitudinal shifts up to 21 km in the mid latitude (Monaghan et al., 2013). This paper performs a series of sensitivity studies where the GISs input layers are

reprojected from spheroid to spherical datum in order to more correctly represent of the input layers used by the atmospheric models.

In a GCS the earth is represented as either an oblate spheroid or a sphere whereas in a spherical system, the earth is always represented as a sphere (Bugayevskiy and Snyder, 1995). This means that when using a spherical coordinate system, the spatial
5   relationships between points on the surface of the earth are altered. The shift in spatial relationship results in a latitudinal error and is consistent across all data that are commonly used as input layers in the atmospheric models such as the Weather Research and Forecasting (WRF) model. Consequently, numerical errors are introduced by computations carried out in WRF that are a function of latitude such as the Coriolis Force and the incoming solar radiation. As already explained in the Monaghan et al. (2013), a minor mismatch between the WRF model global atmosphere input and static variables will affect the simulation
10 result. Figure 1 shows the latitudinal errors introduced when representing a point on the surface of the earth with a spherical GCS. Point A represents data projected on a spheroid system (red line). When that same point A is represented on a sphere (green line) like in an atmospherical model, its location gets incorrectly shifted to the point B. The point C is the true location of the point A when correctly projected in the spherical coordinate system. Figure 2 shows that the errors between spheroid and sphere representation for the same point is a function of latitude. The maximum errors occurs at mid latitude, precisely at
15 45 ° N and S.

Differences in coordinate systems and the resulting spatial errors, such as the example provided in Figure 1, have not been a primary focus in atmospheric modeling because of the relative coarse spatial resolution of the simulation domains (David et al., 2009). More recently, due to the improvements in computational resources and technological advances, atmospheric models are routinely run at higher spatial resolution. Yet this trend in running simulation with high resolution input datasets do not
20 take into account the shift between the coordinate systems which may cause spatial errors in the model's output.

Monaghan et al. (2013) investigated errors caused by different coordinate systems using WRF run with higher resolution topography and land use datasets over Colorado. Multiple WRF simulations were performed to study differences in meteorological parameters such as air temperature, specific humidity and wind speed. They concluded that the GCS transformation from WGS84 GCS to a spherical earth model caused the input data to shift up to 20 km southward in central
25 Colorado. The impact of this shift leads to significant localized effects on the simulation results. The root mean square difference (RMSD) for air temperature is 0.99 °C, for specific humidity is 0.72 g kg^{-1} , for wind speed is 1.20 m s^{-1}. It was concluded that for high resolution atmospheric simulations, the issue resulting from datum and projection errors is increasingly important to solve. All datasets used as input should be in the same GCS (Monaghan et al., 2013).

No study has yet given attention to the impacts of incorrect coordinate systems on the transport of an atmospheric tracer.
30 Sensitivity experiments were conducted to quantify the impact of geographic coordinate systems on the atmospheric mixing ratios of methane (CH_4) emitted from the Marcellus shale gas production activities in Pennsylvania. Using a chemistry module to transport passive tracers in the atmosphere, WRF simulates the CH_4 mixing ratios in the atmosphere.

Geographic information systems and other geospatial technologies have been increasingly used in atmospheric sciences. GIS provides scientific framework for observation data, modelling, and scientific deduction to study atmospheric phenomena
35 and processes (Barkley et al., 2016; Hart and Martinez, 2006; Dobesch et al., 2013). However, some barriers between GIS
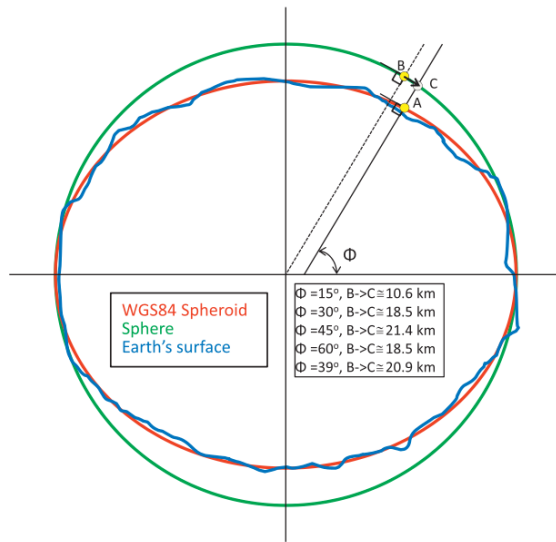
Figure 1. Equivalent points comparisons when using a sphere and spheroid. Blue represents the true earth shape. Green represents the speher that WRF assumes. Red shows the sperhoid WGS84 GCS. Point A represents data projected on a spheroid system. When that same point A is represented on a sphere like in an atomspherical model , its location gets incorrectly shifted to point B. Point C is the true location of point A when correctly projected in the spherical coordinate system. (Monaghan et al., 2013)
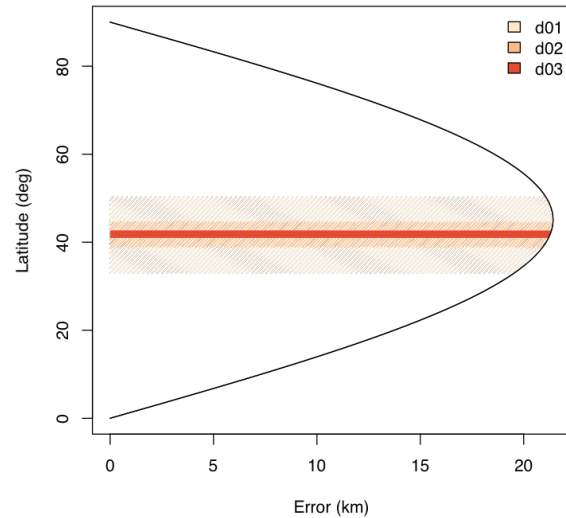
Figure 2. Errors introduced by the different geographic coordinate system are a function of latitude. The maximum error of about 21 km is found at 45 degree latitude. The three shaded areas indicate the latitudinal extents of the three nested WRF domains used in this study.

and atmospheric science, such as different data formats and different GCS, impede the collaborations. This research utilizes the open source language R to make an easy conversion between weather numerical model input and output and GIS data automatically.

The objectives of this study are the following:

1. Quantify the impact of projecting the model input data with different coordinate systems on meteorological variables and simulated atmospheric mixing ratios of a passive tracer.

2. Generate a tool that can automatically convert WRF output to GIS layers and vice-versa.
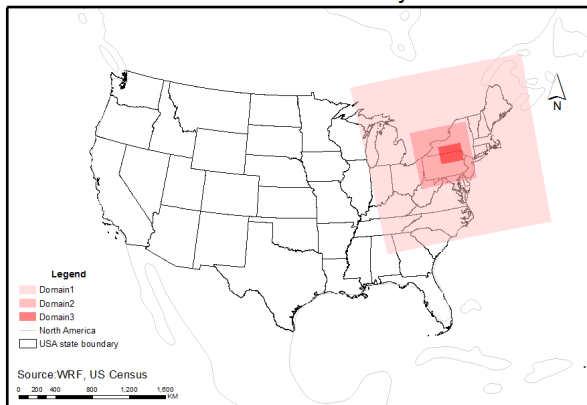
Figure 3. Map of study area shows three nested domains of WRF. The inner domain is located in the north eastern Pennsylvania and extents into Southeast New York.

Figure 4. The elevation in WRF inner domain ranges from 108 m to 761 m. The latitude ranges from 40°N to 42.67°N. The logitude ranges from -78°W to -75.17°W.

2 Study area

The atmospheric simulations were performed using three nested domains of decreasing area and increasing spatial resolutions. As suggested by Monaghan et al. (2013), we defined several criteria to select a region where errors introduced by GCS are more likely to affect our simulation results. First, the region should have larger elevation gradients. Second, it should contain

5   diverse land use patterns such as forest, urban, and wetland. Third, the simulation period requires convective conditions such as summer time since both the topography and the land cover play a larger effect on the simulations. Finally, a comparatively small domain should provide a focused study region because a larger domain would ignore the small variations.

The WRF model grid configuration used in this research contains three nested grids: 9×9 km for domain 1, 3×3 km for domain 2, and 1×1 km for domain 3 (Figure 3). Each 9×9 and 3×3 km grid have a mesh of 202×202 grid points. The 1×1

10   km grid has a mesh of 240×183 grid points.

The 9×9 km grid (domain 1) contains the mid-Atlantic region, the entire northeastern United States east of Indiana, parts of Canada, and a large area of the northern Atlantic Ocean. The 3×3 km (domain 2) grid contains the entire state of Pennsylvania and southern New York. The 1×1 km (domain 3) grid contains northeaster Pennsylvania and southeastern New York. One-way nesting is used so that information from the coarse domain translates to the fine domain but no information from the fine

15   domain translates to the coarse domain (Barkley et al., 2016). The elevation of the domain 3 ranges between 108 and 706 meters above sea level.

The analysis of model results focuses on domain 3. This region was primarily chosen because there has been an increase of activity in natural gas fracking since 2008, which is expected to result in significant releases of fugitive greenhouse gas emissions, in particular CH_4 (Barkley et al., 2016).

3   Data

Variables	DEFAULT scenario	HR scenario	HR_RESHIFT scenario
Topography	USGS	SRTM	SRTM
land use	USGS	NLCD	NLCD
Coriolis	E & F parameters	E & F parameters	E & F parameters
Leaf Area Index	MODIS climatology	8-day MODIS	8-day MODIS
Albedo	MODIS climatology	8-day MODIS	8-day MODIS
CH_4 Emissions	Barkley et al. (2016)	Barkley et al. (2016)	Barkley et al. (2016)

Table 1. The table showing the input data sources for each of the three scenarios(DEFAULT, HR and HR_RESHIFT).

Table 1 shows the input data sources for each of the three scenarios. The variables include topography, land use, Coriolis, Leaf Area Index, Albedo and CH_4 emissions.

3.1   Digital Elevation Data

Two types of elevation data are included in the experiments. The WRF DEFAULT elevation data are derived from the U.S. Geological survey (USGS) Global 30 arc seconds (roughly 900 m) elevation dataset topography, and are used in the DEFAULT case (Gesch and Greenlee, 1996). The HR and HR_SHIFT cases use higher resolution data from the NASA Shuttle Radar Topographic Mission (SRTM) (Farr et al., 2007). The data consist of a 90 m resolution Digital Elevation Model (DEM) for over 80% of the world. The data are projected in a geographic (lat/long) projection with the WGS84 GCS.

3.2   Land Cover Data

The DEFAULT scenario uses the 24 types of land use categories derived from satellite data and are in the WGS84 GCS and are used in the DEFAULT case. The HR and HR_SHIFT cases use the latest landcover products available for Northern America. The 2011 USGS National Land Cover Database (NLCD), covers the continental United States including the state of Alaska and are derived from Landsat satellite imagery with a 30 m spatial resolution. Furthermore, the product is modified from the Anderson Land Cover Classification System and is divided into 20 different land cover types. It has a NAD 1983 GCS and is projected using an Albers conic equal area projection (Homer et al., 2007).

Due to the extent of the NLCD data set, the 2010 North American Land Cover (NALC)[1] is used for the areas of the domain that includes Canada. The NALC product is constructed from observations acquired by the Moderate Resolution Imaging Spectroradiometer (MODIS) at a 250 m spatial resolution. This product is produced by Canada, the US, and Mexico and is represented based on three hierarchical levels using the Food and Agriculture Organization (FOA) Land Classification System.

---

[1]2010 North American Land Cover at 250 m spatial resolution. Produced by Natural Resources Canada/ The Canada Centre for Mapping and Earth Observation (NRCan/CCMEO), United States Geological Survey (USGS); Insituto Nacional de Estadística y Geografía (INEGI), Comisión Nacional para el Conocimiento y Uso de la Biodiversidad (CONABIO) and Comisión Nacional Forestal (CONAFOR)

NALC is based on a sphere GCS with a radius of 6,370,977 m and has a Lambert Azimuthal Equal Area projection (Latifovic et al., 2012).

3.3 Leaf Area Index

The Leaf Area Index (LAI) variable estimates the tree canopy area relative to a unit of ground area (Watson, 1947). Two types
5 of LAI data are used in this experiment. WRF DEFAULT LAI is based on a climatology derived from MODIS is used in the DEFAULT scenario. LAI in HR was obtained from 8-day-averaged data from MODIS. The level-4 MODIS global LAI product composites data every 8 days at 1 km resolution on a sinusoidal grid (NASA LP DAAC, 2015a). The product we used is MCD15A2 for May 2015, which combines the MODIS data from Terra and Aqua satellites.

10 ## 3.4 Albedo

Surface albedo is one of the key radiation parameters required for modeling of the earth's energy budget. In the DEFAULT scenario, albedo use the values from the MODIS modified by National Oceanic and Atmospheric Administration (NOAA) according to green fraction (Chen and Dudhia, 2001).

The HR and HR_RESHIFT cases use the satellite observations that are retrieved from MODIS to produce high-resolution
15 and domain specific albedo input. A 16-Day L3 Global 500 m MCD43A3 product is used for May 2015. The product relies on multiday, clear-sky, atmospherically-corrected surface reflectances to establish the surface anisotropy and provide albedo measures at a 500m resolution (NASA LP DAAC, 2015b).

3.5 CH_4 emissions

CH_4 emission sources include unconventional wells and conventional wells. Both the location and amount of production rate
20 are provided from the Pennsylvania Department of Environmental Protection (PADEP) Oil and Gas Reporting website, New York Department of Environmental Conservation, and the West Virginia Department of Environmental Protection (WVDEP). The emission was calculated by multiplying the production with the emission factors. Omara et al. (2016) indicates that the emission rate for conventional wells is 11% and unconventional well is 0.13% of the well production. The CH_4 emission files were converted as input files for the WRF model (Barkley et al., 2016).

25 ## 3.6 Weather Stations

The weather observations are the standard measurements of wind, temperature and moisture fields from World Meteorological Organization (WMO) surface stations at hourly intervals and radio sondes at 12-houly intervals. The objective analysis program OBSGRID is used for quality control to remove erroneous data (Deng et al., 2009; Rogers et al., 2013). There are 8 stations located in the inner domain. Temperature data during the experiement time from each tower are collected to validate the model
30 simulation results.

4 Methodology

The WRF model (Skamarock and Klemp (2008)) version 3.6.1 is used to generate the numerical weather simulations in this research. It is one of the most widely distributed and used mesoscale Numerical Weather Prediction (NWP) models in existence. It has well-tested algorithms for meteorological data assimilation and meteorological researches and forecast purposes. The WRF model carries a complete suite of atmospheric physical processes that interact with the model's dynamics and thermodynamics core (Barkley et al., 2016).
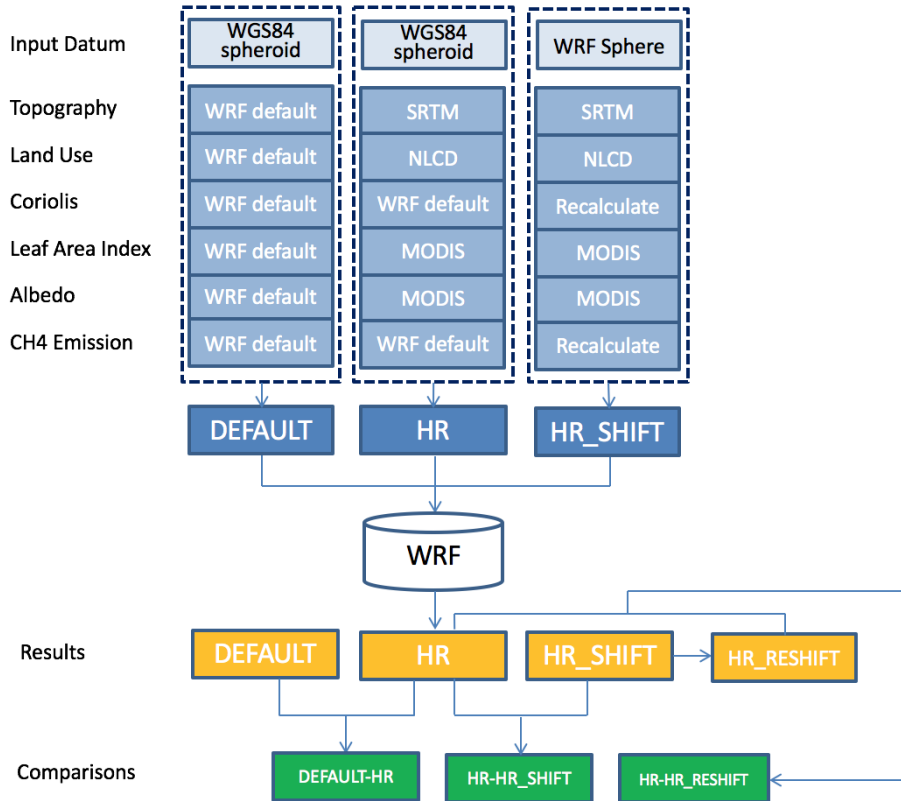
Figure 5. Workflow of the study showing the three scenarios: DEFAULT, HR, HR_SHIFT.

The model physics of the WRF configuration in this research includes the use of the following settings (Barkley et al., 2016). First, the double-moment scheme is used for cloud microphysical processes (Thompson et al., 2004). Second, the Kain-Fritsch scheme is used for cumulus parameterization on the 9-km grid (Kain and Fritsch, 1990; Kain, 2004). Third, the Rapid Radiative Transfer Method is applied to general circulation models (GCMs) (Mlawer et al., 1997; Iacono et al., 2008). Next, the level 2.5 TKE-predicting MYNN planetary boundary layer (PBL) scheme (Nakanishi and Niino, 2006), and the Noah 4-layer land-

surface model (LSM) that predicts soil temperature and moisture in addition to sensible and latent heat fluxes between the land surface and atmosphere are included (Chen and Dudhia, 2001; Tewari et al., 2004; Barkley et al., 2016).

The WRF model enables the chemical transport option within the model allowing for the projection of CH_4 concentrations throughout the domain. Surface CH_4 emissions used as input for the model come from the CH_4 emissions inventory. WRF is able to simulate the CH_4 transport in the atmosphere.

WRF simulations are performed for a 25-hour time period from 07h00 on 14th May 2015 until 07h00 am 15th May 2015 Eastern Standard Time (EST) over the three nested domains described in Section 2. A series of numerical weather simulations were performed using the following input datasets:

1. DEFAULT scenario: DEFAULT WRF topography, land use data, Coriolis E and F, leaf area index, albedo and CH_4 source emissions which are all in WGS84 GCS. The datasets are used as input without applying any transformations into WRF.

2. HR scenario: High resolution terrain and land cover data which are all in WGS84 GCS. The datasets are used as input without applying any transformations into WRF.

3. HR_SHIFT scenario: High resolution terrain, land cover data, Coriolis, leaf area index and albedo data which are first reprojected onto a spherical coordinate system using the transformation function (Hedgley Jr, 1976).

This is a summary of the comparison that are performed to assess the hypothesis.

1. DEFAULT is compared to HR to investigate the impacts on the high resolution input data on model results.

2. HR is compared to HR_SHIFT to investigate the impacts of geographic coordinate system change on model results.

3. HR_RESHIFT is originally the model output from HR_SHIFT simulation. Then, the output is shifted back to WGS84. HR_RESHIFT is compared to HR. These two outputs are in the same geographic coordinate system. The model output comparison, such as temperature, wind speed, wind direction and CH_4 concentration, leads to sensitive understanding of how latitude-dependent variables affect the model simulation.

The input data include elevation, land use, Coriolis E and F components, LAI, albedo and maps of CH_4 sources. The CH_4 sources include conventional wells and unconventional wells. According to Refslund et al. (2013), using high resolution green fraction data does not significantly impact the performance of the weather model simulation. Thus, we did not replace green fractions in this experiment.

The first simulation (DEFAULT scenario) uses the WRF DEFAULT setting: U.S. Geological survey (USGS) Global 30 arc second elevation dataset topography (GTOPO30; Gesch and Greenlee 1996), 24 types land use data, Coriolis parameters E and F, original WRF leaf area index and albedo. In addition to above variables, the experiment takes CH_4 emissions from unconventional and conventional wells as an input to the WRF simulation.

The second simulation, HR, uses higher resolution datasets for terrain, land cover, LAI and albedo. The terrain elevation data are derived from the NASA SRTM Digital Elevation Model (DEM) product at a 90 m resolution. The NALC and NLCD are

used for the land cover data. LAI and albedo are retrieved from MODIS in May 2015. All these data are replaced for all of the three WRF domains. A common approach to re-sample land cover categories to a cell is based on the highest number of pixels that represent a class. Then the highest class occurrence is used to assign the land cover type of the cell. For example if cell A is made up of three different land cover types: 1) Open water 38%, 2) Deciduous Forest 32%, and 3) Evergreen Forest 30%

5   then the final class for cell A would be open water. However, in this work, a hierarchical classification scheme is used to define the land cover type. First, we determine the most common class of land cover types presents inside the cell and create a count order based on the values inside that class. A class corresponds to multiple land cover types. For example, the class "Forest" includes the types "Deciduous Forest" and "Evergreen Forest". We assign the prevalent class, such as Forest, to the given pixel. Second, the grid cell is attributed a land covert type by selecting the type with largest values that are present within a class. For

10   example, if the same cell A is made up of the three different land cover types :1)Open water 38%, 2)Deciduous Forest 32%, and 3)Evergreen Forest 30%, then the final class for cell A would be "Deciduous Forest" because the class "Forest" is most common class (62%) within this cell and "Deciduous Forest" has the highest percentage within the "Forest" class.

The third simulation, HR_SHIFT, uses the same data as the HR scenario, however, the input data are converted from WGS84 to the DEFAULT WRF sphere GCS.

15   Coriolis is a function of latitude and thus particularly affected by errors in GCS. Coriolis force has two components, E and F are calculated using $E = 2\Omega sin(\varphi)$ and $F = 2\Omega cos(\varphi)$ where Ω is rotation rate of the earth and φ represents latitude. Coriolis E and F variables are recalculated in the HR_SHIFT scenario by using the reprojected latitude.

Experiment ID	Input GCS	Output GCS
DEFAULT	WGS84	WGS84
HR	WGS84	WGS84
HR_SHIFT	WRF Sphere	WRF Sphere
HR_RESHIFT	WRF Sphere	WGS84

Table 2. shows the input and output GCS for the data used in each of the four analysis that will be performed.

Table 2 shows the input and output GCS for the topographic, land use, and CH$_4$ data used for the WRF simulations. Specifically, results discuss the output for the DEFAULT and HR, and HR and HR_RESHIFT configurations. A prototype

20   tool is developed to automatically transfer WRF output to GIS layers.

5   WRF model input and output processing

A series of scripts in R are provided to perform the tasks identified in the current paper. Figure 6 shows the process used to generate new input data based on additional input data and an optional coordinate transformation. This process is performed in the WRF_preprocess.R and WRF_updateNC.R scripts. WRF_process.R takes WRF original input files as input and shift the

25   selected WRF layers to sphere raster format. In addition, users generate an ESRI Shapefile as an output. WRF_UpdateNC.R

file takes the generated Rdata files, and updates them into the original WRF input file. The detailed descriptions are attached in appendix.
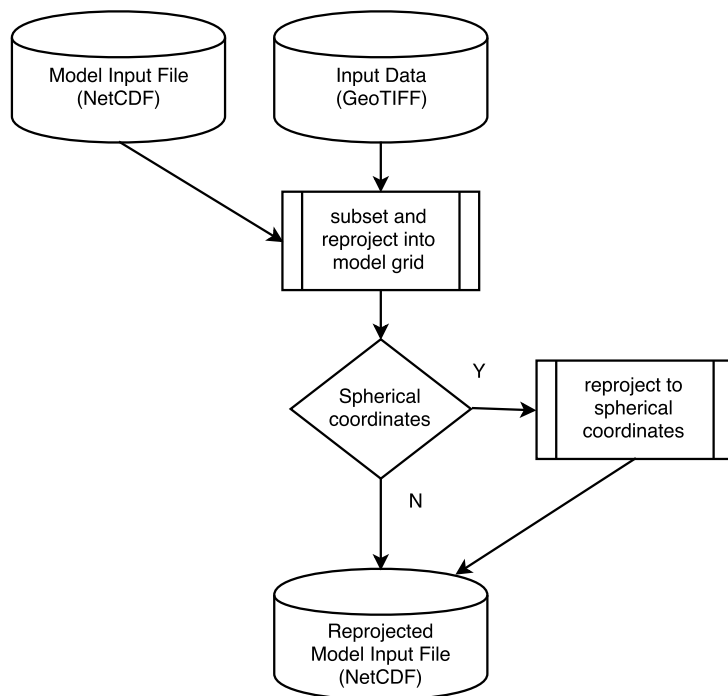
Figure 6. Flowchart for transforming and generating new model input data

Additional scripts are provided to perform basic transformation of the input data from their original format to the lat-long WGS84 format that is used by WRF_preprocess.R to generate new model input data. For example MODIS_LAI.R is used to automatically download and reproject MODIS satellite data in a format that can be input into the WRF input file. These functions are provided to automate the process of downloading and reprojecting MODIS data, the same results can be achieved through several already alternatively methodologies. Essentially, the MODIS functions are wrappers around the MODIS Reprojection Tool, which is provided by NASA (NASA, 2017).

The current code assumes standard WRF input data in NetCDF format, however the script can be easily modified to accept a different input format from a model other than WRF.

6 Results

The WRF model is used to simulate the atmospheric dynamics between May 14th, 2015 07h00 and May 15th 2015 07h00 EST. This work focuses on four output variables produced during the WRF simulation: air temperature, mean horizontal wind speed
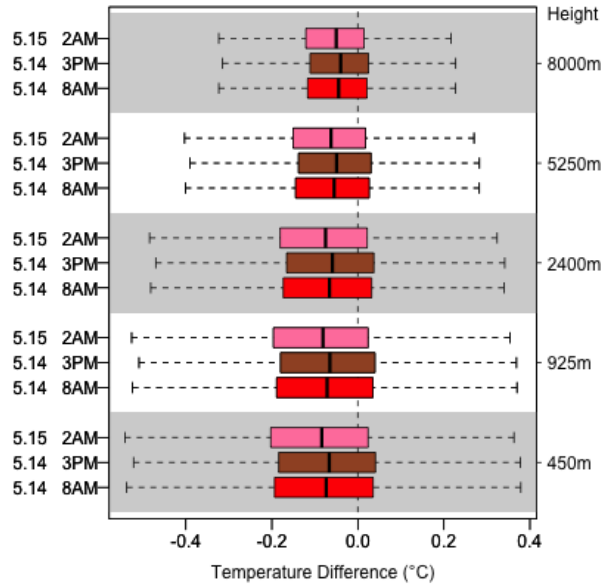
Figure 7. Temperature differences between HR and DEFAULT in the domain 3.
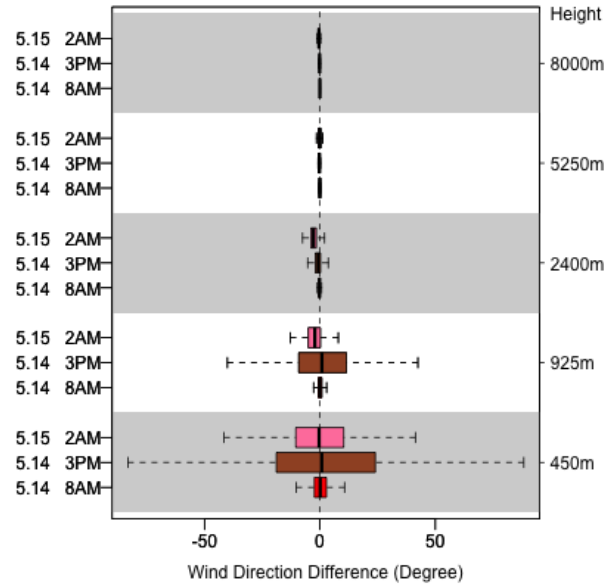
Figure 8. Wind direction differences between HR and DEFAULT in the domain 3.
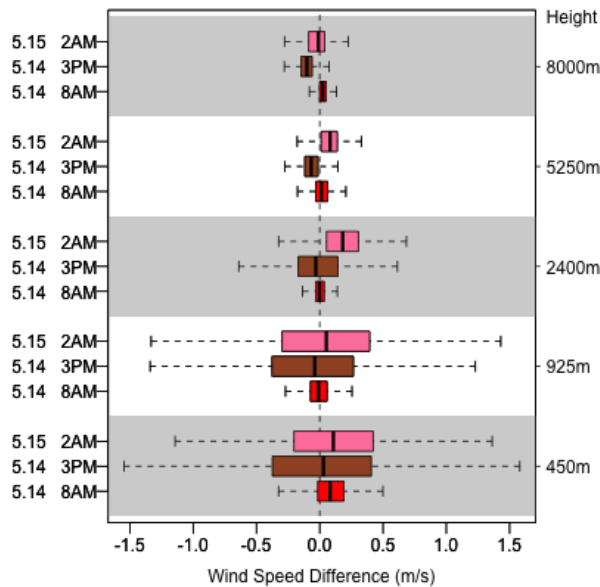
Figure 9. Wind speed differences between HR and DEFAULT in the domain 3.
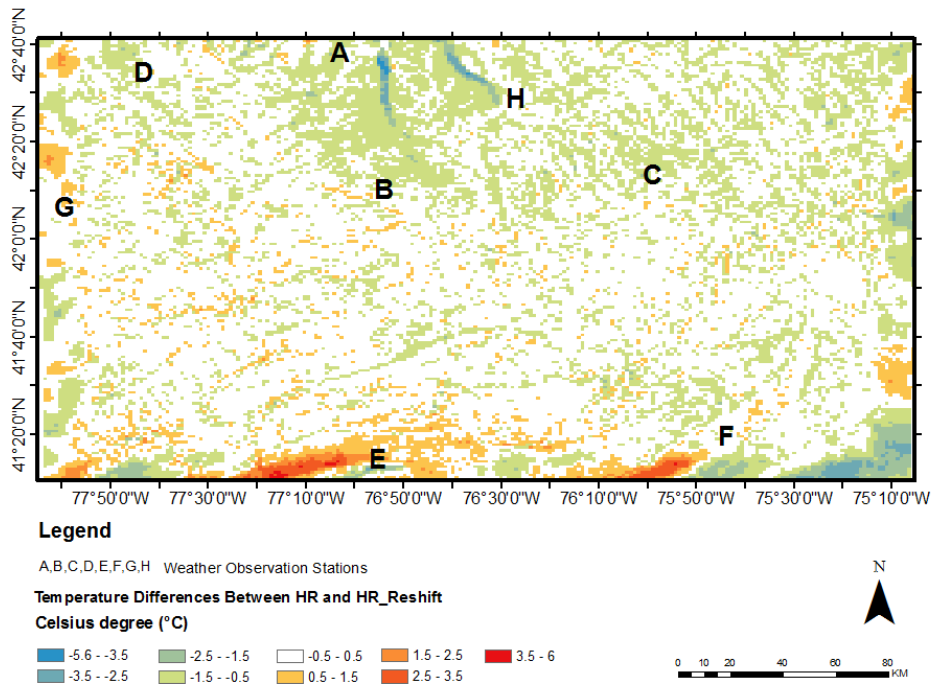
Figure 10. Temperature difference between HR and HR_RESHIFT on May 14th 15h00, 2015 showed that there is no significant spatial pattern.

and direction, and CH$_4$ atmospheric mixing ratios. Temperature was selected because it is one of the main drivers of local and large scale weather. Additionally historical temperature data are available for comparison purposes. Near-surface temperature also corresponds to areas of higher energy which relates to turbulent motions near the surface as well as surface water exchange (evaporation). Wind speed and wind direction were selected to represent the atmospheric dynamics impacting the weather

5   conditions at small and large scales. Finally, we selected the CH$_4$ mixing ratios to quantify the impact on greenhouse gas transport in the atmosphere.

6.1   DEFAULT and HR Sensitivity Study

Previous studies have investigated the weather simulation performance differences by using higher resolution data. While the comparison between DEFAULT and HR is not the central focus of this work, experiments were performed to confirm previous

10   findings, and to quantify changes due to using higher resolution vs changes due to the different GCSs.

     Figure 7, 8 and 9 compare the WRF simulations for domain 3 for temperature, wind direction and wind speed respectively. The figures show that using higher resolution data does not significantly alter the results obtained using the DEFAULT WRF input.
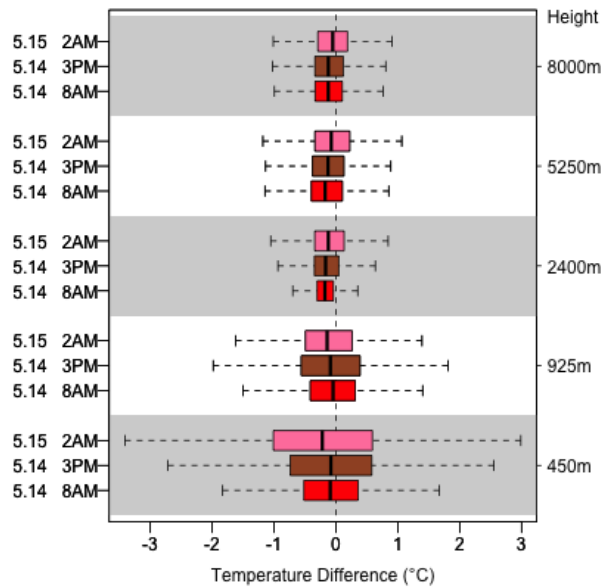
Figure 11. Temperature differences between HR and HR_RESHIFT in domain 2.
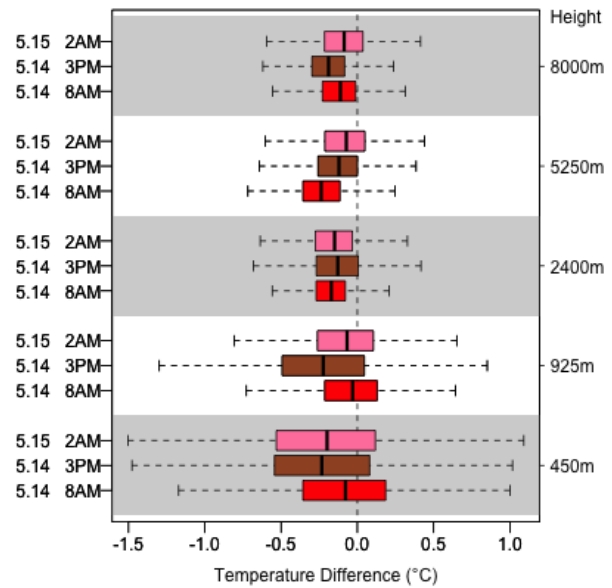
Figure 12. Temperature differences between HR and HR_RESHIFT in domain 3.

6.2 HR and HR_RESHIFT Sensitivity Study

This section analyzes the main hypothesis of the article, namely investigating the effect of using a different geographic coordinate system on the simulations of temperature, wind speed, wind direction and CH_4 mixing ratio.

6.2.1 Results for Temperature

5 The effect of using a different coordinate system on the simulations of temperature is performed by comparing observations between the un-shifted (HR) and shifted (HR_SHIFT) scenarios. Figure 10 shows the difference obtained for May 14th, 2015 at 15h00. This particular time and day were chosen because it is one of the hottest times of the day, when temperature are expected to vary the most. Letters A - H represent the eight weather observation stations located inside the selected domain and are used for validation purposes.

10 The temperature difference ranges from -5.6 °C represented by light blue colors to 6 °C shown with orange/red colors. When comparing both HR and HR_RESHIFT, the most striking spatial pattern is the systematic cooling around the finger lakes (roughly bound by points A, B and H). There are several additional areas of increased positive and negative temperature around the perimeter of the image, where most extremes are observed. However, these are likely to be artifacts introduced by the WRF computations where the nested grids meet. The largest differences are observed at the edges of the domain, and are

15 likely artifacts being introduced by WRF where the nested grids change resolutions.
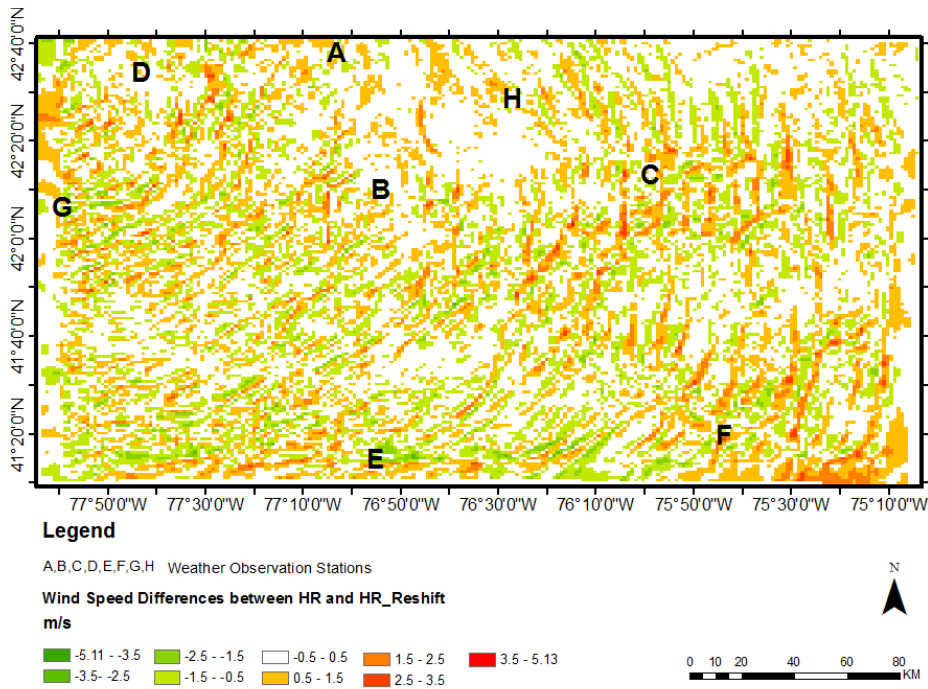
Figure 13. Wind speed difference between HR and HR_RESHIFT on May 14th 15h00, 2015 showed a wave pattern.

Statistical tests were performed using the observed weather data (stations A-H), and both scenarios (HR and HR_RESHIT) have a 0.91 root mean square error. While this suggests that there are only small temperature variations when using a different GCS, it should be noted that this test was performed only at eight stations throughout the domain where ground data were available. Unfortunately, several of these stations lie close at the edge of the domain, where WRF simulation results are most

5   unreliable. Therefore, the spatial cooling observed around the lakes is the most important results obtained entirely due to the change in GCS.

Both domain 2 and domain 3 show a systematic temperature increase in the HR_RESHIFT scenario when compared to HR (Figure 11 and Figure 12). The height is represented on the vertical axis while the temperature difference is on the horizontal axis. The variability and mean temperature differences are larger near the surface and below 1 km altitude. This

10   height corresponds approximately to the average boundary layer height where the impact of the surface on the atmospheric dynamics is maximum. The variability in the mid Troposphere decreases significantly, revealing a lower impact of the GCS on the higher altitude model results.

6.2.2 Results for Wind speed

Figure 13 shows the wind speed difference for May 14th, 2015 at 11h00, which ranges from -5.11 to 3.5 m s^{-1} between HR and

15   HR_RESHIFT. A wave pattern is found during the 25 hours simulation, and it can be explained by the shifted data allowing for
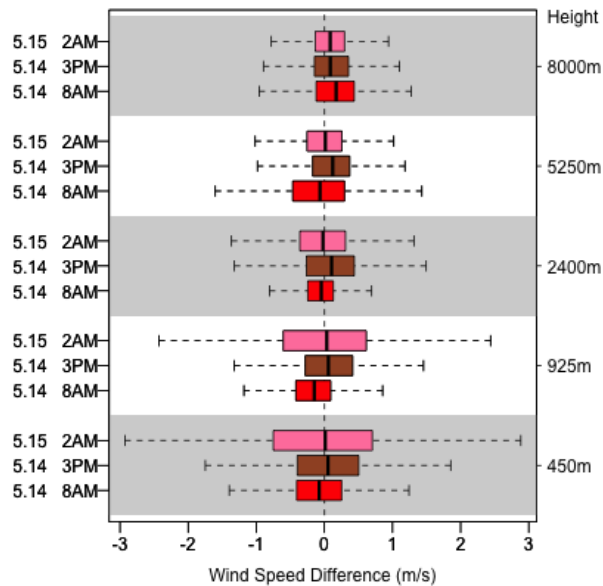
Figure 14. Wind speed differences between HR and HR_RESHIFT in the domain 2.
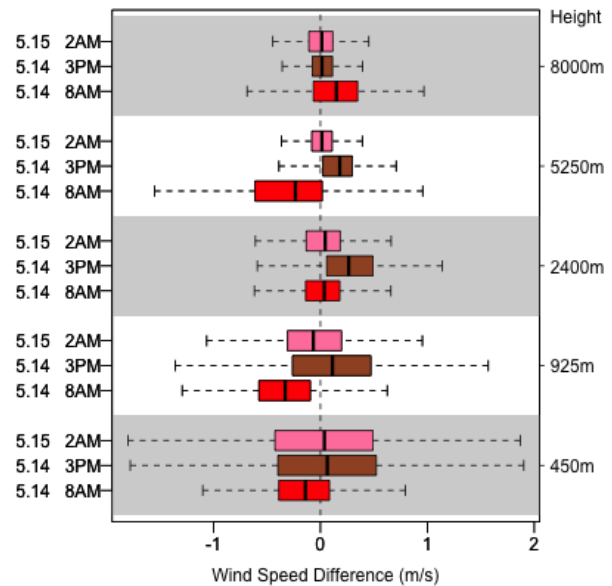
Figure 15. Wind speed differences between HR and HR_RESHIFT in the domain 3.

a more accurate characterization of the complex terrain along the Appalachian mountains. The wind speed differences between HR and HR_RESHIFT indicate that the change in GCS affects the results.

6.2.3 Results for Wind direction

Figure 18 and Figure 19 show results for wind directions, and point out that, as for the previous cases, the most differences are found closer to the surface. As explained earlier, changes in GCS affect the interaction in the lower layers of the troposphere the most .

In the northeastern corner of the inner domain, there is a strip-like pattern, with large local wind changes between positive and between positive and negative North-East and North-West, and South-East and South-West. In this region the Appalachian mountains create a complex terrain with series of valley and ridges. The GCS changes the spatial distribution of the terrain elevation, leading to these very large changes in wind direction The strong vertical gradients observed in the figure suggest there there is also a combination of influences from both the surface parameters (primarily elevation and land cover), and the Coriolis components. Despite observed changes throughout the vertical column, the near-surface variability is significantly larger than the mid-Tropospheric variances as observed for temperature and wind speed.

6.2.4 Results for CH$_4$ Atmospheric Mixing Ratios

WRF was used to simulate CH$_4$ atmospheric mixing ratios originated from leaks from unconventional and conventional natural gas production activities respectively during the 25 hours simulation. CH$_4$ mixing ratio is a unique tracer to study atmospheric
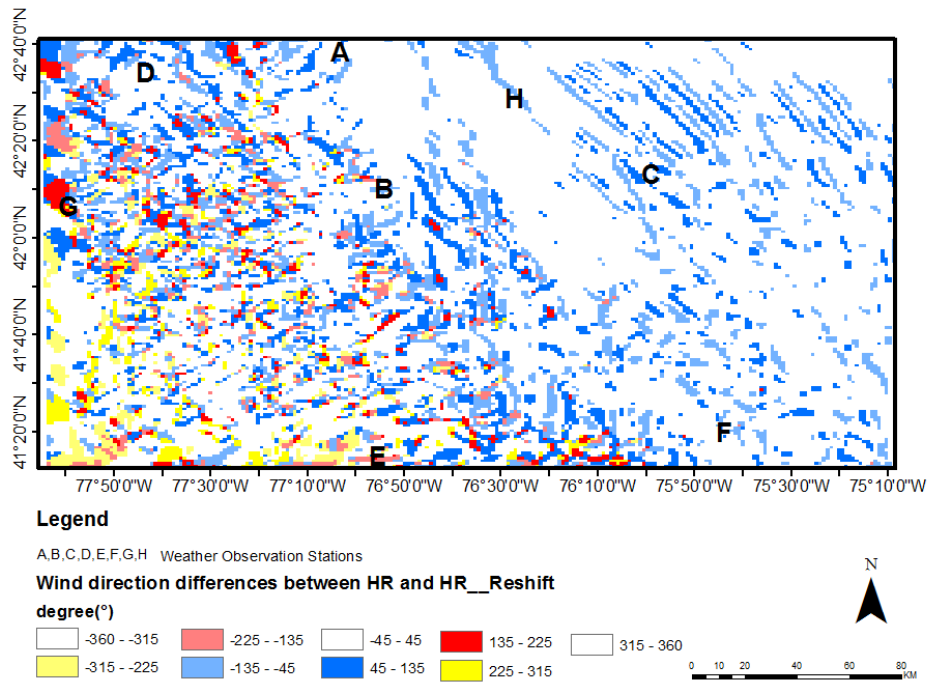
Figure 16. Wind direction difference between HR and HR_RESHIFT on May 14th 15h00, 2015 showing a strip pattern in the right top corner where it is a valley region. The pattern indicates that WRF model reacts differently on a small area weather simulation when the GCS changes.
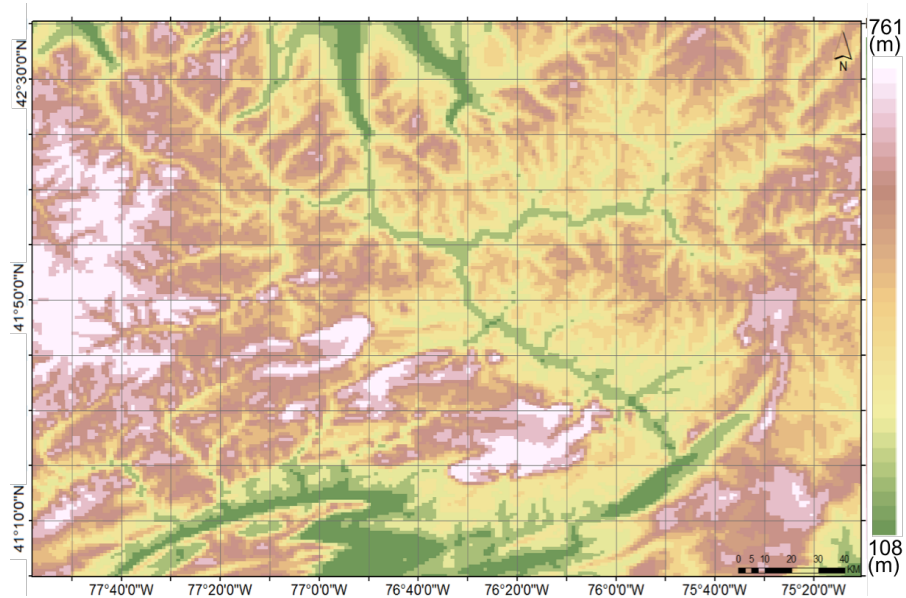
Figure 17. Domain 3 topography map. The elevation ranges from 108 m to 761 m above the sea level.
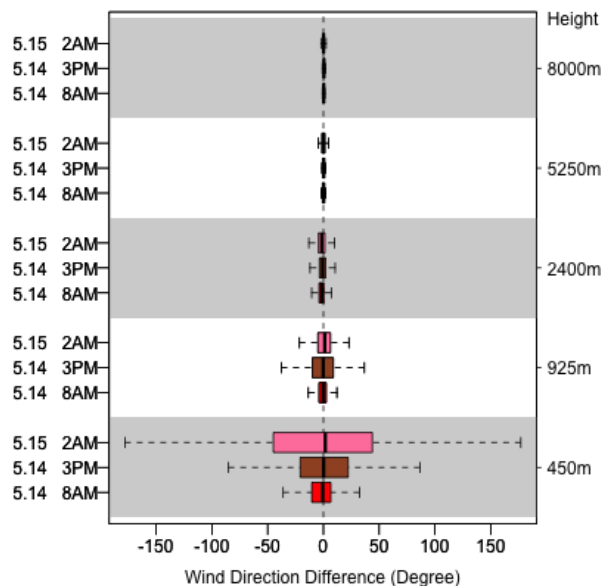
Figure 18. Wind direction differences between HR and HR_RESHIFT in the domain 2.
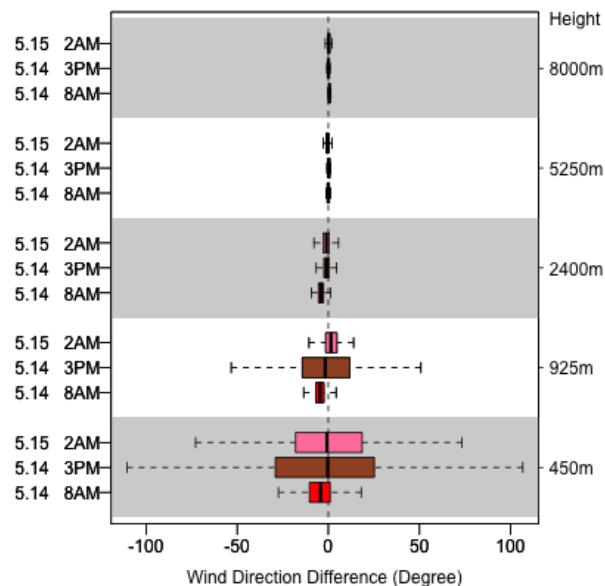
Figure 19. Wind direction differences between HR and HR_RESHIFT in the domain 3.

dynamics and well suited for this experiment because domain 3 includes the northeastern Pennsylvania which, since 2008, has became one of the most important fracking area in the United States since 2008. With the development of fracking, the CH_4 leaks became a concern because CH_4 has a Global Warming Potential (GWP) between 28 to 36 during 100 years. It means that the comparative impact of CH_4 on climate change is 28 to 36 times greater than CO_2 over a 100-year period (US EPA, 2015).

5   CH_4 mixing ratios are computed differently than temperature, wind speed and wind direction. Temperature, wind speed and wind directions are computed using global atmospheric input data, which is an internal variable of the WRF model physics. On the other hand, CH_4 mixing ratios are computed solely on the CH_4 emissions created using multiple datasets. Thus, CH_4 mixing ratios were selected to investigate the impact of differences in GCS on the simulation accuracy aggregated over time, as CH_4 accumulates differences along its trajectories in the atmosphere. Overall, we expect a strong sensitivity to transport
10   differences revealed by the long range transport of CH_4 emitted at the surface. Figure 20 and Figure 21 show the mean of CH_4 mixing ratios differences between HR and HR_RESHIFT for conventional and unconventional wells as a function of time. The figure show two radar plots, where the times have been arranged as on a clock. The left image indicates the results for AM and the right image for PM. When the shade area is larger than 0, CH_4 mixing ratios in HR is larger than it in HR_RESHIFT, and vise versa.

15   For conventional wells (Figure 20), the differences are often close to 0, with night time increases (21h00 to 04h00). For the unconventional wells (Figure 21), CH_4 mixing ratio in HR is also smaller during night time (21h00 to 08h00), but much more so (as much as 1 PPB smaller). The reason for this change is because during night time the mixing within the boundary layer is smaller (more stable atmosphere) and therefore the magnitude of the concentration of CH_4 are higher. Because of the higher
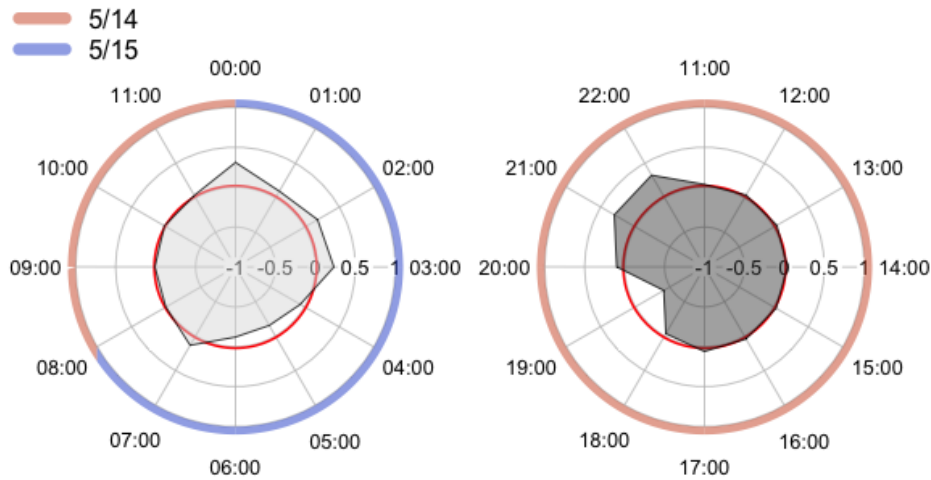
Figure 20. CH$_4$ mixing ratios difference between HR and HR_RESHIFT in Domain 3 for conventional wells. Left figure shows the morning time differences including 01h00 to 12h00 in May 14th and May 15th. The right figure shows the afternoon until midnight differences between 13h00 to 24h00 in May 14th.
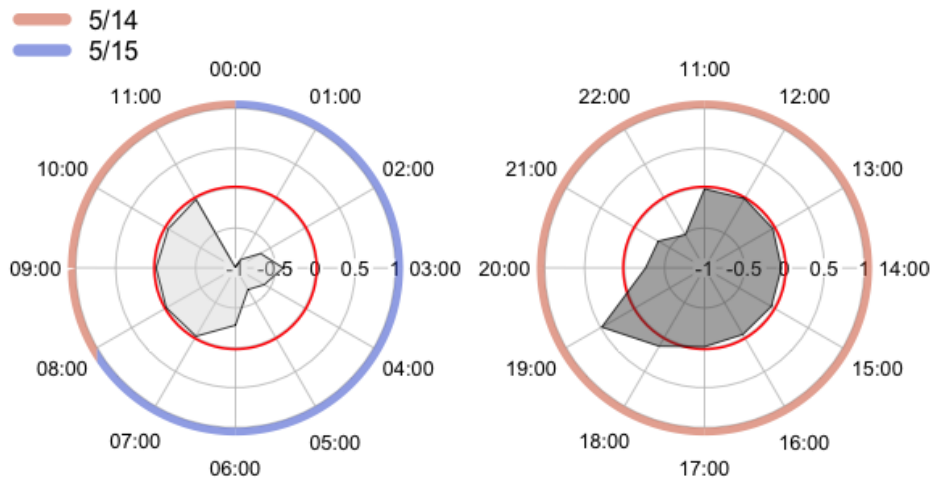
Figure 21. CH$_4$ mixing ratios difference between HR and HR_RESHIFT in Domain 3 for Unconventional wells. Left figure shows the morning time differences including 01h00 to 12h00 in May 14th and May 15th. The right figure shows the afternoon until midnight differences between 13h00 to 24h00 in May 14th.

concentrations, the impact of the change in GCS is bigger. Furthermore, the explanation as to why conventional wells have a smaller variation that unconventional wells is because most of them are are located farther away from the tower network, and thus their emission contribution on the simulation is smaller because distributed over a wider area. These results show a significant change in the CH$_4$ mixing ratio when using the different GCS.

7 Conclusions

This paper discusses the impact of different geographic coordinate system on weather numerical model simulations. The main hypothesis is that the error introduced by not taking into account the GCS of the input data, which result in latitudinal errors of up to 21 km in the mid latitudes, can cause significant changes in the output of the model.

A sensitivity study was performed using the WRF numerical model, with input data at different resolutions and different GCSs. Four different output parameters were investigated, namely temperature, wind speed, wind direction and CH_4 mixing ratios.

Results show that changes are introduced by using different GCSs for the input data. The observed differences were caused by 1) topography shift including elevation, land use, albedo, LAI differences; and 2) latitude-dependent physics, such as the Coriolis force and the incoming solar radiation.

A systematic temperature increase was observed in all of the three domains used in this study. A spatial pattern showing significant cooling was observed near two lakes included in the inner domain.

Similarly, wind speed and direction show spatial changes that can be traced back to the use of a different land cover and elevation. Wind speed, wind direction and temperature indicate more variations within the planetary boundary layer where the interaction between the surface and the atmosphere is greatest. It is expected that changes at the surface will introduce most significant changes closer to the surface.

It is shown that, without exceptions, the GCS of the input data affects model results. Sometimes these changes are large and have a clear spatial patterns, whereas other times are small and negligible. It is concluded that while some of of these errors might be small, they nevertheless introduce an additional bias in the model output. Especially for very high resolution simulation, these errors are compounded and can lead to significant errors.

While it is best to properly project all data in the correct representation used by the model, which in the case of WRF is a spherical GCS, it is most important to keep the GCS and projection among the input layers consistent. In fact, if all layers are in the same GCS, errors in mapping onto the surface of the earth are consistent across the datasets and the effect of using the wrong GCS are minimized. On the other hand, mixing GCSs in the input data leads to larger errors.

8 Code availability

WRF processing code is available at https://github.com/yannicao/wrf_reprojection.

9 Acknowledgments

This research was partially supported by the Department of Energy (DE-FE0013590) and by the Office of Naval Research (ONR) award #N00014-16-1-2543 (PSU #171570)

References

Barkley, Z., Davis, K., Lauvaux, T., Miles, N., Richardson, S., Martins, D., Deng, A., Cao, Y., Sweeney, C., Karion, A., Smith, M., Kort, E., and Schwietzke, S.: Quantifying methane emissions from natural gas production in northeastern Pennsylvania, 2016.

Bugayevskiy, L. M. and Snyder, J.: Map projections: A reference manual, CRC Press, 1995.

Chen, F. and Dudhia, J.: Coupling an advanced land surface-hydrology model with the Penn State-NCAR MM5 modeling system. Part I: Model implementation and sensitivity, Monthly Weather Review, 129, 569–585, 2001.

David, C. H., Gochis, D. J., Maidment, D. R., Yu, W., Yates, D. N., and Yang, Z.-L.: Using NHDPlus as the Land Base for the Noah-distributed Model, Transactions in GIS, 13, 363–377, 2009.

Deng, A., Stauffer, D., Gaudet, B., Dudhia, J., Hacker, J., Bruyere, C., Wu, W., Vandenberghe, F., Liu, Y., and Bourgeois, A.: Update on WRF-ARW end-to-end multi-scale FDDA system, 23, 2009.

Dobesch, H., Dumolard, P., and Dyras, I.: Spatial interpolation for climate data: the use of GIS in climatology and meteorology, John Wiley & Sons, 2013.

Farr, T. G., Rosen, P. A., Caro, E., Crippen, R., Duren, R., Hensley, S., Kobrick, M., Paller, M., Rodriguez, E., Roth, L., et al.: The shuttle radar topography mission, Reviews of geophysics, 45, 2007.

Gesch, D. and Greenlee, S.: GTOPO30 documentation, US Department of the Interior US Geological Survey. Accessed January, 24, 2012, 1996.

Hart, J. K. and Martinez, K.: Environmental Sensor Networks: A revolution in the earth system science?, Earth-Science Reviews, 78, 177–191, 2006.

Hedgley Jr, D. R.: An exact transformation from geocentric to geodetic coordinates for nonzero altitudes, 1976.

Homer, C., Dewitz, J., Fry, J., Coan, M., Hossain, N., Larson, C., Herold, N., McKerrow, A., VanDriel, J. N., Wickham, J., et al.: Completion of the 2001 national land cover database for the counterminous United States, Photogrammetric Engineering and Remote Sensing, 73, 337, 2007.

Iacono, M. J., Delamere, J. S., Mlawer, E. J., Shephard, M. W., Clough, S. A., and Collins, W. D.: Radiative forcing by long-lived greenhouse gases: Calculations with the AER radiative transfer models, Journal of Geophysical Research: Atmospheres, 113, 2008.

Kain, J. S.: The Kain–Fritsch Convective Parameterization: An Update, Journal of Applied Meteorology, 43, 170–181, 2004.

Kain, J. S. and Fritsch, J. M.: A one-dimensional entraining/detraining plume model and its application in convective parameterization, Journal of the Atmospheric Sciences, 47, 2784–2802, 1990.

Latifovic, R., Homer, C., Ressl, R., Pouliot, D., Hossain, S., Colditz, R., Olthof, I., Giri, C., and Victoria, A.: North American land change monitoring system, Remote sensing of land use and land cover: principles and applications, pp. 303–324, 2012.

Mlawer, E. J., Taubman, S. J., Brown, P. D., Iacono, M. J., and Clough, S. A.: Radiative transfer for inhomogeneous atmospheres: RRTM, a validated correlated-k model for the longwave, Journal of Geophysical Research: Atmospheres, 102, 16 663–16 682, 1997.

Monaghan, A. J., Barlage, M., Boehnert, J., Phillips, C. L., and Wilhelmi, O. V.: Overlapping Interests: The Impact of Geographic Coordinate Assumptions on Limited-Area Atmospheric Model Simulations, Monthly Weather Review, 141, 2120–2127, 2013.

Nakanishi, M. and Niino, H.: An improved Mellor–Yamada level-3 model: Its numerical stability and application to a regional prediction of advection fog, Boundary-Layer Meteorology, 119, 397–407, 2006.

NASA: https://lpdaac.usgs.gov/tools/modis_reprojection_tool_swath, [Accessed 2017-03-22], 2017.

NASA LP DAAC: Leaf Area Index Fraction of Photosynthetically Active Radiation 8 Day L4 Global 1km. NASA EOSDIS Land Processes DAAC, USGS Earth Resources Observation and Science (EROS) Center, Sioux Falls, South Dakota (https://lpdaac.usgs.gov), https://lpdaac.usgs.gov/dataset_discovery/modis/modis_products_table/mcd15a2, accessed June 27 2016, 2015a.

NASA LP DAAC: LAlbedo 16-Day L3 Global 500m. NASA EOSDIS Land Processes DAAC, USGS Earth Resources Observation and
5   Science (EROS) Center, Sioux Falls, South Dakota (https://lpdaac.usgs.gov), https://lpdaac.usgs.gov/dataset_discovery/modis/modis_products_table/mcd43a3, accessed June 1 2016, 2015b.

Omara, M., Sullivan, M. R., Li, X., Subramanian, R., Robinson, A. L., and Presto, A. A.: Methane Emissions from Conventional and Unconventional Natural Gas Production Sites in the Marcellus Shale Basin, Environmental science & technology, 50, 2099–2107, 2016.

Refslund, J., Dellwik, E., Hahmann, A. N., and Boegh, E.: Updated vegetation information in high resolution WRF simulations, Iahs-aish
10   Publication, pp. 233–238, 2013.

Rogers, R. E., Deng, A., Stauffer, D. R., Gaudet, B. J., Jia, Y., Soong, S.-T., and Tanrikulu, S.: Application of the Weather Research and Forecasting model for air quality modeling in the San Francisco Bay area, Journal of Applied Meteorology and Climatology, 52, 1953–1973, 2013.

Skamarock, W. C. and Klemp, J. B.: A time-split nonhydrostatic atmospheric model for weather research and forecasting applications,
15   Journal of Computational Physics, 227, 3465–3485, 2008.

Tewari, M., Chen, F., Wang, W., Dudhia, J., LeMone, M., Mitchell, K., Ek, M., Gayno, G., Wegiel, J., and Cuenca, R.: Implementation and verification of the unified NOAH land surface model in the WRF model, pp. 11–15, 2004.

Thompson, G., Rasmussen, R. M., and Manning, K.: Explicit forecasts of winter precipitation using an improved bulk microphysics scheme. Part I: Description and sensitivity analysis, Monthly Weather Review, 132, 519–542, 2004.

20 US EPA, C. C. D.: Methane Emissions, http://epa.gov/climatechange/ghgemissions/gases/ch4.html, [Accessed 2015-05-01], 2015.

Watson, D. J.: Comparative physiological studies on the growth of field crops: I. Variation in net assimilation rate and leaf area between species and varieties, and within and between years, Annals of Botany, 11, 41–76, 1947.

Appendix A: WRF_preprocess.R

The signature for the function is as follows:

WRF.preprocess(filename.wrf,

filename.raster,

WRF.layer,

shift.to.sphere,

write.shapefile,

cores)

where:

- filename.wrf is the input file that contains the original WRF input files.

- filename.raster is the filename for the new data (e.g. MODIS LAI) file that is being used to replace the original WRF input.

- WRF.layer is the layer name in the WRF input file. For example HGT represents the height, F and E the coriolis latitudinal and meridional components.

- shift.to.sphere is a boolean (TRUE or FALSE) and determines if the input raster is reprojected to spherical coordinates from the original lat long WGS84.

- write.shapefile is a boolean (TRUE or FALSE) and determines if an ESRI Shapefile is generated.

- cores specifies the number of cores for parallel processing.

Appendix B: WRF_UpdateNC.R

WRF_UpdateNC.R file takes the generated Rdata files, and updates them into the original WRF input file.

The signature for the function are as follows:

load(filename.data)

put.var.ncdf(WRF.new,

WRF.layer,

WRF.data.HR)

where:

- filename.data is the Rdata generated from WRF.preprocess.

– WRF.new is an object of class ncdf.

– WRF.layer is what variable to write the data to. They could be HGT_M, LU_INDEX , F, E, LAI12M, and ALBEDO12M.

– WRF.data.HR is the values to be written.